Draft version May 10, 2007
Preprint typeset using LaTeX style emulateapj v. 7/15/03



# OUTFLOWS AND THE PHYSICAL PROPERTIES OF QUASARS

Rajib Ganguly[1], Michael S. Brotherton[1], Sabrina Cales[1], Brian Scoggins[1], Zhaohui Shang[1,2], Marianne Vestergaard[3]

*Draft version May 10, 2007*

## ABSTRACT

We have investigated a sample of 5088 quasars from the Sloan Digital Sky Survey Second Data Release in order to determine how the frequency and properties of broad absorptions lines (BALs) depend on black hole mass, bolometric luminosity, Eddington fraction ($L/L_{Edd}$), and spectral slope. We focus only on high-ionization BALs and find a number of significant results. While quasars accreting near the Eddington limit are more likely to show BALs than lower $L/L_{Edd}$ systems, BALs are present in quasars accreting at only a few percent Eddington. We find a stronger effect with bolometric luminosity, such that the most luminous quasars are more likely to show BALs. There is an additional effect, previously known, that BAL quasars are redder on average than unabsorbed quasars. The strongest effects involving the quasar physical properties and BAL properties are related to terminal outflow velocity. Maximum observed outflow velocities increase with both the bolometric luminosity and the blueness of the spectral slope, suggesting that the ultraviolet luminosity to a great extent determines the acceleration. These results support the idea of outflow acceleration via ultraviolet line scattering.

*Subject headings:* quasars: general — quasars: absorption lines — quasars: fundamental parameters

## 1. INTRODUCTION

The nature and significance of broad absorption lines (hereafter, BALs) seen in some 10-20% of high luminosity quasars is still not apparent. The broad, blueshifted lines indicate that high velocity outflows are present in at least some quasars. The outflows are potentially important as they may enable accretion through carrying away angular momentum, and they may significantly chemically enrich the interstellar medium of the quasar host galaxy and the surrounding intergalactic medium.

There are a number of potential explanations for observed frequency of BALs. In the interest of unified schemes, it is postulated that all high-luminosity quasars host the outflows that give rise to BALs. This postulate is not without warrant, as quasars with and without BALs appear to show similar intrinsic observed continuum and emission-line properties (e.g., Weymann et al. 1991; Gallagher et al. 1999). In its simplest interpretation, the frequency of observed BALs is tied to the covering factor of the outflow around the central black hole. That is, whether or not one observes the outflow in absorption depends on the orientation of the central engine (e.g., Weymann et al. 1991; Goodrich 1997; Krolik & Voit 1998). Early evidence from spectro-polarimetry of BALs bolstered the idea that BAL quasars were viewed edge-on (or nearly so) and the outflow was equatorial (e.g., Goodrich & Miller 1995). This explanation is difficult to reconcile in the face of new evidence from the studies of radio-loud BALs. The discovery of radio-loud BAL quasars (e.g., Becker et al. 2000) opens up the possibility of directly gauging the orientations of BALs. Mounting evidence in the form of spectro-polarimetry and brightness temperatures (e.g., Brotherton et al. 2006, and references therein) is showing that BALs are viewed at a large variety of viewing angles (from $\sim 15°$ from the jet axis to nearly edge-on).

Two plausible alternative explanations include unification in the time-domain or more complicated orientation schemes. The former case purports that BALs are a short-duration (possibly episodic) phase in the duty cycle of the accreting black hole (e.g., Voit, Weymann, & Korista 1993; Becker et al. 2000; Gregg et al. 2000; Gregg, Becker, & de Vries 2006). Such a scenario also tends to connect BALs to even rarer objects like post-startburst quasars (e.g., Brotherton et al. 1999) and to more extreme objects ultra-luminous infrared galaxies (e.g., Sanders et al. 1988) in suggestive evolutionary sequences.

In the latter case, the geometry of the outflow, and hence the frequency with which it is intercepted producing a BAL, is dependent on the intrinsic SED (or physical parameters) of the disk. For instance, in the conventional wisdom, the physical parameters that are most strongly tied to the presence of a BAL outflow is the Eddington ratio and the black hole mass (e.g., Boroson & Green 1992; Boroson 2002; Proga & Kallman 2004). Boroson (2002) and Yuan & Wills (2003) have shown that BAL quasars have strong Fe II and weak [O III] emission putting them at one extreme of the Boroson & Green (1992) Eigenvector 1, which is thought to be driven to the accretion rate in Eddington units. In this scheme, BAL quasars are thought to be the more massive (hence, more luminous) analogs of narrow-line Seyfert 1 galaxies (e.g., Brandt & Gallagher 2000; Boroson 2002).

After many decades of work, we now have the means to reliably estimate the fundamental physical properties (e.g., black hole mass, bolometric luminosity, Eddington ratio) of a quasar. Thus, we are in a position to ask whether (and how) the parameters of a BAL outflow de-

[1] Department of Physics and Astronomy, University of Wyoming (Dept. 3905), 1000 East University Ave., Laramie, WY 82072
[2] Department of Physics, Tianjin Normal University, 300074 Tianjin, China
[3] Department of Astronomy and Steward Observatory 933 N Cherry Ave., Tucson AZ 85721-0065

TABLE 1. CLASSIFICATION OF SDSS-DR2 $1.7 \leq z \leq 2$ QUASARS

| | Pre-Fitting | | Post-Fitting | |
|---|---|---|---|---|
| Class | Number | Fraction | Number | Fraction |
| LoBALs | 55 | 1% | ... | |
| mini-BALs/BALs | 562 | 11.0% | 536 | 10.5% |
| AALs | 1898 | 37.3% | 1813 | 35.6% |
| Unabsorbed | 2573 | 50.6% | 2509 | 49.3% |
| Total | 5088 | | 4858 | 95.5% |

NOTE. — The columns on the left indicate our subjective classifications before applying our fitting prescriptions to measure the Mg II emission line region. The columns on the right indicate the number of quasars that had reasonable fits. Bad fits were typically due to poor S/N, or the presence of intervening or associated absorption contaminating the Mg II emission line.

pend on the physical quasar properties. With the large numbers of quasars available through the Sloan Digital Sky Survey, we can do so in a highly statistically significant manner, where only systematic uncertainties affect our results. Our approach here is to address and answer some of these questions about BAL quasars by determining their fundamental physical properties and comparing them to normal quasars (i.e., to make differential comparisons where systematics should not affect the result) and to look for correlations with BAL properties. We explain the details of our methodology in §2, our basic results in §3, discuss the results in §4, and summarize our conclusions in §5. We adopt a cosmology with $\Omega_M = 0.3$, $\Omega_\Lambda = 0.7$, $H_0 = 70\,\mathrm{km\,s^{-1}\,Mpc^{-1}}$ throughout this paper.

## 2. DATA AND METHODS

### 2.1. *Selection and Classification*

Our sample comes from the Sloan Digital Sky Survey (SDSS; York et al. 2000), Data Release 2 (DR2; Abazajian et al. 2004). We requested all 5088 objects classified as having broad emission lines, i.e., quasars, with redshifts between 1.7 and 2.0. This redshift range places both the C IV $\lambda$1549 and Mg II $\lambda$2800 emission lines in the window of the SDSS spectra (which covers the range $\sim$3820–9200 Å). The C IV region permits us to identify BALs, while the Mg II region can be used to make virial mass estimates (McLure & Jarvis 2002). The BAL absorption associated with C IV makes that line a bad choice for making mass estimates. When BALs are found associated with low-ionization species like Al III $\lambda$1860, and Mg II, then the Mg II line is also compromised much of the time. This measurement is required for black hole mass estimation, which in turn is needed to determine the Eddington luminosity. In addition, low-ionization BAL quasars appear systematically reddened compared to other quasar classes (e.g., Sprayberry & Foltz 1992; Yamamoto & Vansevičius 1999; Becker et al. 2000; Najita et al. 2000; Brotherton et al. 2001; Hall et al. 2002; Richards et al. 2003; Reichard et al. 2003a), making the determination of the continuum luminosity more uncertain and probably biased unless an uncertain correction is made. Therefore, we have excluded low-ionization BAL quasars from our subsequent analysis (leaving 5033 total objects). We make an additional cut below when we fit the Mg II region of the spectra.

We subjectively classify objects (i.e., through visual inspection) into three classes: (1) objects displaying clear signs of an outflow (mini-BALs/BALs); (2) objects showing no signs of intrinsic absorption (Unabsorbed); and (3) objects that have absorption near the C IV emission line that may break up into discrete components at higher resolution (AALs[4]). The incidence of each of these classes in listed in the second and third columns of Table 1. In our subjective scheme, we adhere to the idea that an outflow seen in absorption should be relatively smooth (i.e., that the profile is unlikely to break up into more discrete components if observed at higher dispersion). If a profile appears too clumpy (i.e., consists of narrow components), then it is placed in the AAL class, if the absorption takes place near the emission line. If the absorption has a narrow velocity dispersion (FWHM $\lesssim$500 km s$^{-1}$), is clumpy and appears at a large blueshift, it is taken to result from intervening structures (which typically is also accompanied by narrow low-ionization absorption lines). Since there is likely a continuum of velocity widths that arise from absorption by outflows, there will be a cases where our classification is incorrect. To combat this, four of the authors (Ganguly, Brotherton, Cales, and Scoggins) have independently classified the spectra. Comparison between the authors leads to very few cases where there is any dispute, implying that our classifications are both uniform and reproducible. Using only a single-epoch low-dispersion spectrum, we feel that this is the best that can be accomplished without resorting to more quantitative schemes. [Such schemes would require continuum-fitting procedures, such as template fitting or polynomial fitting, and are beyond the scope of this investigation.]

While our classifications are subjective, we feel they are more complete than the various quantitative schemes from the literature which are either insufficient, biased, or too contaminated with false-positives for our purposes. The BALnicity Index (BI) was defined by Weymann et al. (1991) in order to be sure they classified only BAL quasars as BAL quasars with low signal-to-noise ratio and low-resolution LBQS spectra. For example, intrinsic absorption systems that appear at high velocity (i.e., mini-BALs) can be excluded when using a BI criterion. Intrinsic absorption appearing within 5000 km s$^{-1}$ would also be excluded by a BI selection. Similarly, the Absorption Index (AI) of Hall et al. (2002)[5], while more liberal than the BI, still has some fairly arbitrary limits to help weed out blends of associated absorbers that may be intervening systems. Since we wish to test the properties of outflows (e.g., maximum velocity of absorption, onset velocity, velocity width) as a function of other quasar properties (e.g., luminosity, black hole mass), it is important that our sample be roughly complete. We emphasize here that absorption by outflows comes from a continuum of velocity widths. While a small error rate in our classifications would not compromise our study,

[4] The AAL abbreviation stands for "associated" absorption lines. Nominally, these are lines that have a narrow velocity-dispersion ($\lesssim$ 500 km s$^{-1}$) and appear near the quasar redshift ($c|\Delta z| \lesssim 5000$ km s$^{-1}$). We do not adhere strictly to these criteria in our subjective classification scheme. C IV absorption that is narrow or sufficiently clumpy and appears superposed on the C IV emission line is deemed an AAL.

[5] See Trump et al. (2006) for a revised definition of this parameter.

Table 2. Comparison to Trump et al. (2006) Classification Scheme

| | Total | Unabs. | AALs | BAL | LoBAL |
|---|---|---|---|---|---|
| This Work | 5088 | 2572 | 1898 | 562 | 55 |
| T06, AI> 0 | 1206 | 181 | 420 | 551 | 54 |
| T06, AI≤ 0 | 3882 | 2391 | 1478 | 11 | 1 |
| Breakdown of Trump et al. (2006) AI> 0 classes | | | | | |
| high-ionization | 1158 | 178 | 400 | 540 | 40 |
| low-ionization | 48 | 3 | 20 | 11 | 14 |
| Hi | 835 | 72 | 186 | 537 | 40 |
| nHi | 321 | 106 | 214 | 1 | 0 |
| H | 2 | 0 | 0 | 2 | 0 |
| Lo | 41 | 3 | 16 | 10 | 12 |
| nLo | 3 | 0 | 1 | 1 | 1 |
| LoF | 3 | 0 | 2 | 0 | 1 |
| nLoF | 1 | 0 | 1 | 0 | 0 |

Note. — T06 indicates Trump et al. (2006). The fourth row, labeled "high-ionization," denotes the sum of the "Hi," "nHi," and "H" classifications. The fifth row, labeled "low-ionization," denotes the sum of the "Lo," "nLo," "LoF," and "nLoF" classifications. See text for a description of the sub-classes.

inclusion of only BI>0, or AI>0 objects in a sample of objects with outflows would bias our results.

We compare our subjectively-selected sample to the more objective BAL quasar sample from the SDSS third data release compiled by Trump et al. (2006). In total, we find that 562 of the 5088 objects in our sample appear to have spectroscopic evidence of high-ionization outflowing gas (i.e., with no accompanying low-ionization absorption). By comparison, 1206 of the 5088 objects appear in the Trump et al. (2006) BAL catalog with the following classifications: Hi – 835, nHi – 321, H – 2, Lo – 41, nLo – 3, LoF – 3, nLoF – 1. [A "Hi" or "H" classification indicates the presence of C IV absorption, while a "Lo" classification indicates the additional presence of Mg II absorption. An "n" prefix indicates that the absorption width is narrow while a "F" indicates the presence of Fe II absorption.] That is, Trump et al. (2006) appear to find 1158 objects with evidence for high-ionization outflows. At face value, it would seem that our subjective classification scheme is not more efficient at selecting outflows. We present a cross-comparison of our classification scheme and that of Trump et al. (2006) in Table 2. In the first two rows of the table, we present a head-to-head comparison of the total number objects in our work and those objects that would have been flagged as BALs by Trump et al. (2006), as well as the breakdown with our classifications. In the next two rows (rows three and four), we further break down the Trump et al. (2006) numbers by ionization. In the remaining rows of the table, we present the full demographics using the Trump et al. (2006) classification and their comparison with our classification scheme. We draw the reader's attention to the following comparisons:

1. Of the 562 quasars with high-ionization outflows (BALs) that we selected, Trump et al. (2006) only cataloged 551 objects. Of these, only 540 have a "Hi," "nHi," or "H" classification. The other 11/551 objects (that are in the catalog) are given "Lo" or "nLo" classifications. The 11/562 objects that are not in the Trump et al. (2006) catalog are shown in Figure 1. Of these, six are cases where either the velocity limits of integration for AI or the continuous absorption criterion are not sufficient. In other cases, the profile may be too shallow relative to the signal-to-noise to allow a precise AI measurement.

2. 181 of the objects classified by Trump et al. (2006) as a BAL appear to be intrinsically unabsorbed objects, typically with Mg II or Fe II absorption by intervening structures. Examples of these objects are shown in Figure 2.

3. 40 of the objects that we classify as LoBALs are presented as HiBALs in the Trump et al. (2006) catalog. These objects appear either somewhat reddened or have broad absorption near the Mg II or Al III emission lines, which may affect our ability to carry out spectral fits of the Mg II region.

4. For 400 of the objects classified by Trump et al. (2006) as high-ionization BAL quasars ("Hi" or "nHi"), it is not clear that the C IV absorption is necessarily a result of an outflow. In these cases, the absorption profiles seem as if they would break into more discrete components if observed at higher resolving power. The gas may be due to absorption by the host galaxy, or other structures related to the quasar/quasar environment. We place these objects in our AAL class.

We also note that 1478 additional quasars in our sample have AALs, that is narrow velocity-dispersion systems appearing within 5000 km s$^{-1}$ of the quasar redshift. Some of these are likely to be intrinsic to the quasar central engine in some form. [Estimates range from $\geq 20\%$ (Wise et al. 2004) based on time-variability to $\sim 33\%$ based on partial coverage (Misawa et al. 2007).] None of these systems were found with the revised AI-based selection scheme of Trump et al. (2006).

We conclude that, in this sample, the number of objects with outflows detectable in absorption is probably closer to our value of 562 (11%), and has likely been overestimated (through the inclusion of "false positives") in the Trump et al. (2006) catalog. While the efforts at quantitatively selecting outflows are undergoing revision (and have certainly progressed from the days of BALnicity), further revisions are required to decrease the number of false-positives. If our assessments are taken to be a truer reflection of outflow classifications, then we estimate that the Trump et al. (2006) catalog is 98% (605/617) complete toward finding HiBALs and LoBALs (consistent with their estimation), but suffers a 15% (181/1206) rate of false-positives. Detailed scrutiny of subsamples of sources, such as presented here, should help in that goal.

### 2.2. *Spectral Fitting and Parameter Estimation*

Since one of our goals is to compare the physical properties (e.g., continuum luminosity, spectral shape, virial mass, Eddington ratio) of absorbed and unabsorbed quasars, we carried out fits around the Mg II $\lambda$2800 emission line (over the rest-frame wavelength range 2000–3000 Å) using the SPECFIT task (Kriss 1994). Our fits include a power-law continuum (with the convention

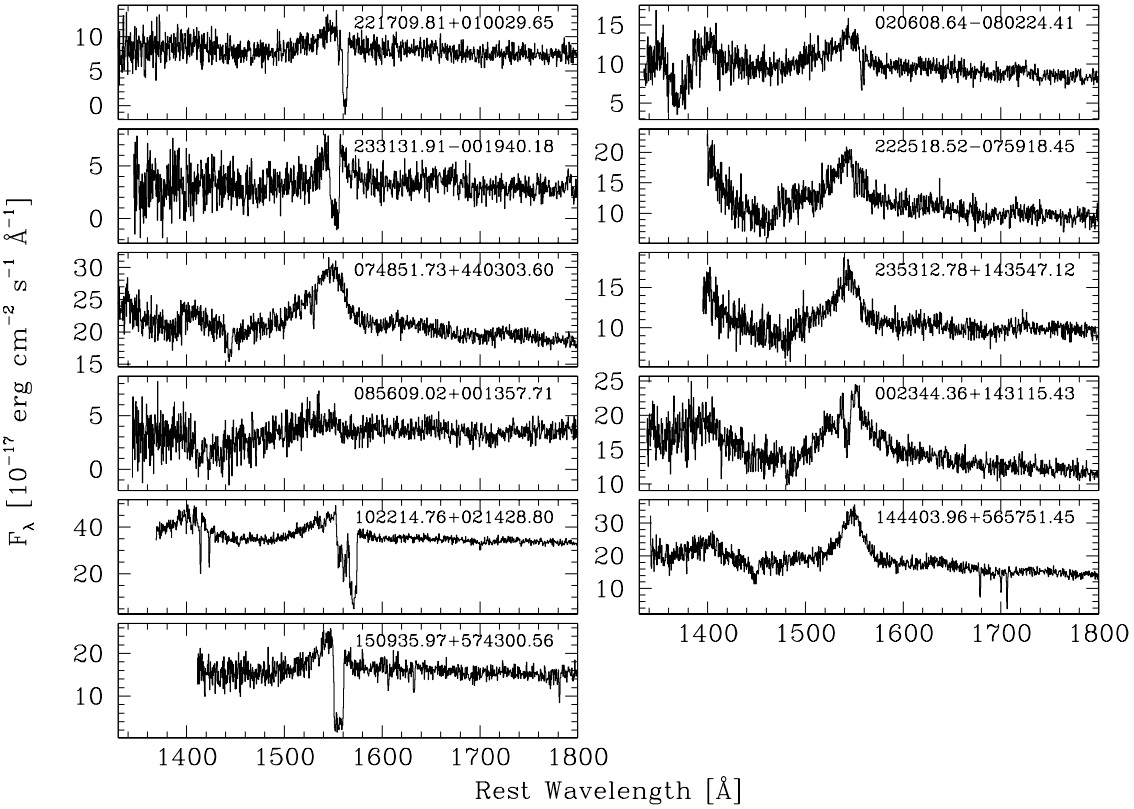


FIG. 1.— We show spectra of the 11 objects that we subjectively classify as HiBALs, that do not appear in the Trump et al. (2006) catalog.

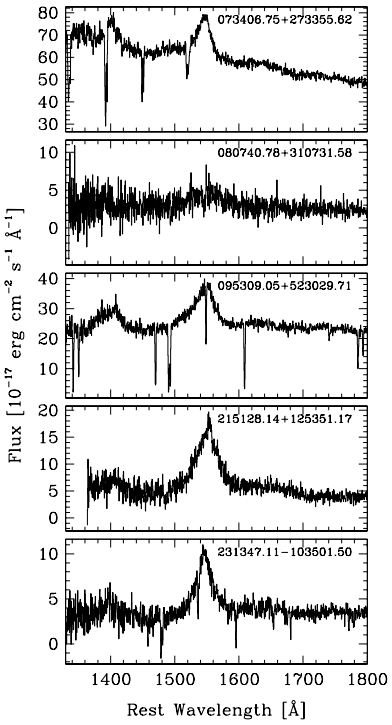


FIG. 2.— We show example spectra of objects selected by Trump et al. (2006) as HiBALs which do not appear to show intrinsic absorption by our subjective classification.

$F_\lambda \sim \lambda^{-\alpha}$), the I Zw 1 iron emission template (Vestergaard & Wilkes 2001), and two Gaussians (a broad and a narrow component) for the Mg II emission line. The fits were carried out on spectra that were reduced to rest-frame wavelengths calculated using the redshift reported by SDSS.

Initially, we tried to fit all spectra with a single fitting prescription (as summarized in column 3 of Table 3). We found that there was sufficient variety in the spectra that one prescription was not adequate, and we turned to five different prescriptions. These five prescriptions are also summarized in Table 3, which includes allowed ranges in the parameters, and parameters that were tied together. For example, in one prescription, we tied the wavelength shifts of the broad and narrow Mg II components and the Fe II together (i.e., no relative shift between them). In another prescription, all three shifts were allowed to vary independently. We also tried prescriptions with different ranges in various parameters like the magnitude of the shifts or the widths of the emission line components.

We took the approach of fitting each spectrum using the all five prescriptions and adopting the model that provided the best fit (i.e., the lowest $\chi^2$ value). The bottom four rows of the table report the number of times each prescription was adopted for all quasars and for the three quasar classes (mini-BALs/BALs, AALs, Unabsorbed). In many cases, more than one prescription provides a good fit, with similar best-fit values and the actual difference in $\chi^2$ values is small. In all, we were able to achieve good fits for about 95% of the quasar

Table 3. Summary of Fitting Prescriptions

| Property | Unit | Run Number 1 | 2 | 3 | 4 | 5 |
|---|---|---|---|---|---|---|
| Power-law | | | | | | |
| Index[a] | | [1,10] | [0.1,10] | [0.1,3] | [0.1,3] | [0.1,3] |
| Normalization[b] | | [1,10000] | [0.1,10000] | [0.1,10000] | [0.1,10000] | [0.1,10000] |
| Fe template | | | | | | |
| Scaling | | [0.001,10] | [0.001,10] | [0.001,10] | [0.001,10] | [0.001,10] |
| Wavelength shift | Å | 0 | M2B | [-50,50] | 0 | [-50,50] |
| Width | km s$^{-1}$ | [900,10000] | [900,12000] | [900,12000] | [900,12000] | [900,12000] |
| Mg II broad component | | | | | | |
| Scaling | | [0.1,10] | [0,30000] | [0,30000] | [0,30000] | [0,30000] |
| Wavelength shift | Å | [-28,22] | [-28,22] | [-18,22] | [-18,22] | [-98,102] |
| Width | km s$^{-1}$ | [2000,20000] | [2000,20000] | [2000,20000] | [2000,20000] | [2000,20000] |
| Mg II narrow component | | | | | | |
| Scaling | | [0.1,10] | [0,30000] | [0,30000] | [0,30000] | [0,30000] |
| Wavelength shift | Å | [-18,22] | M2B | M2B | M2B | M2B |
| Width | km s$^{-1}$ | [900,10000] | [900,10000] | [900,10000] | [900,10000] | [900,10000] |
| Number of times chosen: | | 711 | 1687 | 1693 | 735 | 32 |
| mini-BALs/BALs: | | 65 | 141 | 233 | 92 | 5 |
| AALs: | | 269 | 644 | 609 | 271 | 20 |
| Unabsorbed: | | 377 | 902 | 851 | 372 | 7 |

Note. — In all cases, the fits were carried out on the rest-frame wavelength range 2000–3000 Å. M2B: The parameter was tied to the same value as the corresponding parameter of the Mg II broad component.
[a]The sign convention for the power-law index, $\alpha$, is $F_\lambda \sim \lambda^{-\alpha}$.
[b]Units for the power law are $10^{-17}$ erg cm$^{-2}$ s$^{-1}$ Å$^{-1}$

spectra. 230 of the quasars could not be fit well due to poor signal-to-noise, or the presence of intervening or associated absorption contaminating the Mg II emission line. In the right two columns of Table 1, we report how many quasars in each classification were successfully fit with one of our prescriptions. Comparison of these numbers with the pre-fitting numbers indicates that no single class was affected more than the others.

We show in Figure 3 a comparison of fitted properties (near UV spectral index, 3000 Å luminosity, and Mg II $\lambda$2800 emission line FWHM) between three of our quasar classes, unabsorbed quasars, BAL quasars, and AAL quasars. We numerically computed the Mg II $\lambda$2800 emission line FHWM from the sum of the two Gaussian components. Generally there is good agreement between the samples with, perhaps, the mini-BAL/BAL class having systematically broader Mg II $\lambda$2800 emission-lines, flatter spectral indices, and higher 3000 Å luminosities.

From the fitting parameters, we estimate two fundamental physical properties for all the quasars, the black hole mass, and the Eddington ratio. For an estimation of the black hole mass for each quasar, we use the following prescription derived by McLure & Jarvis (2002) which uses the 3000 Å monochromatic luminosity and the Mg II $\lambda$2800 FWHM:

$$\frac{M_{\rm BH}}{M_\odot} = 3.37 \left( \frac{\lambda L_\lambda (3000\,\text{Å})}{10^{42} \text{erg s}^{-1}} \right)^{0.47} \left[ \frac{\text{FWHM(MgII)}}{\text{km s}^{-1}} \right]^2 \quad (1)$$

Dietrich & Hamann (2004) note that this scaling law gives about a factor of five smaller mass than estimates based on the C IV or H$\beta$ emission line widths (e.g., Kaspi et al. 2000). However, since our primary goal is to look at *differences* in quasar properties between BALs and non-BALs, this should not adversely affect our results.

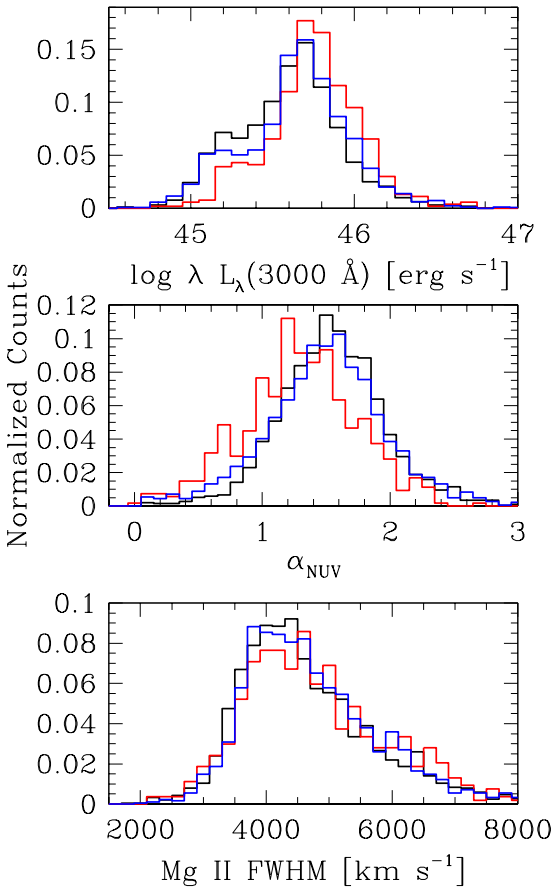


Fig. 3.— We compare the continuum fitting results between BAL QSOs (red or dark histogram), Unabsorbed QSOs (black or shaded histogram), and AAL QSOs (blue or light histogram). The distributions have been normalized to unit area.

Table 4. Outflow Absorption-Line Measurements

| Target | BI (km s$^{-1}$) | $v_{\rm min}$ (km s$^{-1}$) | $v_{\rm max}$ (km s$^{-1}$) |
|---|---|---|---|
| SDSS J002344.36+143115.43 | 0 | 6964 | 27697 |
| SDSS J020608.64−080224.41 | 0 | 32771 | 39285 |
| SDSS J074851.73+440303.60 | 0 | 15421 | 25505 |
| SDSS J085609.02+001357.71 | 0 | 16512 | 28419 |
| SDSS J102214.76+021428.80 | 0 | -4933 | 587 |
| SDSS J150935.97+574300.56 | 0 | -2107 | -103 |
| SDSS J144403.96+565751.45 | 0 | 19375 | 23666 |
| SDSS J220900.66−001413.23 | 425 | 1469 | 6677 |
| SDSS J222518.52−075918.45 | 0 | 15453 | 24780 |
| SDSS J233131.91−001940.18 | 0 | -2090 | 193 |
| SDSS J235312.78+143547.12 | 0 | 1022 | 26929 |

We estimate the bolometric luminosity identically for each quasar. The measured rest-frame flux at 3000 Å from the fit to the power-law continuum is converted into an emitted luminosity using luminosity distances for our cosmology. We convert these monochromatic luminosities into bolometric luminosities:

$$L_{\rm bol} = 4\pi D_{\rm L}^2 f (1+z) \lambda F_\lambda, \quad (2)$$

where $\lambda = 3000$ Å, $F_\lambda$ is the observed flux density at 3000 Å, $D_{\rm L}$ is the luminosity distance, and $f = 5$ is the average bolometric correction from 3000 Å (see Figure 12 from Richards et al. 2006). We acknowledge here that other, and perhaps more refined, estimates of the bolometric correction (e.g., Vestergaard 2004; Shang et al. 2005). Use of these estimates would generally require an extrapolation of our power-law fit to another wavelength, which we wish to avoid. Since we are making a differential comparison between BAL and non-BAL quasars, this should not affect our results. Richards et al. (2006) estimate ∼20% uncertainty in using a mean bolometric correction. This would have the effect of smearing out the distribution. In the absence of yet more refined approaches to making bolometric corrections *en masse*, we feel this is best that can be done.

We calculate the Eddington luminosity for each quasar given our estimate of the mass of its black hole: $L_{\rm Edd} = 1.51 \times 10^{38} (M/M_\odot)$ erg s$^{-1}$ (e.g., Krolik 1999, eq. 6.21). We then compute the Eddington ratio, $L_{\rm bol}/L_{\rm Edd}$. In Table 7, we present our measurements of these quasars, as well as the two derived physical parameters (black hole mass, Eddington ratio), the fitting run that provided the best fit, and our classification.

In addition to measurements of the continuum and emission-line properties of the quasar, we also wish to test how BAL properties depend on quasar properties. The Trump et al. (2006) catalog already presents various measurements for most (but not all) of our BALs. We adopt the BALnicity index (BI), absorption index (AI), and maximum velocity of absorption ($v_{\rm max}$) measurements from Trump et al. (2006) for the 551 BALs that appear in their catalog. For the remaining 11 BAL quasars that do not appear in the Trump et al. (2006) catalog, we use our measurements of BI and $v_{\rm max}$. These are listed in Table 4 (as well as the onset velocity of absorption, $v_{\rm min}$). We did not measure AI values for the 11 BAL quasars because the new definition of AI to reflect a true equivalent width requires knowledge of the (uncertain) shape of the C IV emission-line since the integration range starts at zero velocity. Trump et al. (2006) use a sophisticated template-fitting algorithm to reproduce the emission-line shapes, but this is beyond of the scope of this paper. A comparison of our BI and $v_{\rm max}$ measurement methods to those of Trump et al. (2006) for a subsample of BALs indicates that the two are consistent.

## 3. ANALYSIS

### 3.1. *Differences Between BAL and Non-BAL Quasars*

With measurements/derivations of the quasar physical properties, we can explore if there are systematic differences between unabsorbed quasars and BAL quasars. The distributions of measured properties (Figure 3) do not show appreciable differences in either the general shape or in the mean values (Table 5). BAL quasars may be systematically more luminous (at 3000 Å) and have redder NUV spectra ($\langle\alpha({\rm BAL})\rangle = 1.29$, $\langle\alpha({\rm Unabs.})\rangle = 1.55$, with standard deviations of $\sim 0.4$), but only slightly . We note here that the absolute shape of the luminosity distribution is affected by the SDSS quasar selection criteria. The important observation here is that there does not appear to be qualitatively significant *differences* between the three quasar classes (Unabsorbed, AALs, and BALs); they are all within a standard deviation.

Quantitative tests (like the Kolmogorov-Smirnov test) do show that the small differences in the distributions are apparently significant. However, when dealing with such large samples, even small differences in the distributions can be manifest as having high statistical significance. We stress here that visual inspection of Fig. 3-4 show very clear overlaps, and quite similar shapes, between the three classifications in the distributions of all parameters.

Figure 4 shows a comparison of the distribution of Eddington ratios, black hole masses, and bolometric luminosities for the three samples of quasars (BALs, AALs, and Unabsorbed); mean values for those quantities are reported in Table 5. While the distributions imply that BAL quasars have systematically larger bolometric luminosities than unabsorbed quasars, the distribution of the Eddington ratios for those two samples are quite similar extending down to very small values ($L_{\rm bol}/L_{\rm Edd} \lesssim 0.1$). This is a rather profound result given the expectation from the analysis of Palomar-Green quasars that BALs should have higher than normal accretion rates, since BAL quasars in the PG sample lie at one extreme of the Boroson & Green (1992) Eigenvector 1. In the conventional interpretation, Eigenvector 1 is taken to be driven by the Eddington ratio (e.g., Boroson 2002).

One factor that could affect the robustness of this result is the average bolometric correction of BAL quasars from 3000 Å. If indeed the spectral shape of BAL quasars is different from unabsorbed quasars, one can question the validity of using the same (or similar) bolometric correction. If the mean bolometric correction for BAL quasars are, for example, higher by factor of $\sim 2$, then the mean Eddington ratio would be of order unity. However, even if this were the case, we would still have a significant number of BAL quasars with relatively small Eddington ratios, given the broad distribution in Fig. 4.

Regardless, at best it is not clear if the average bolometric correction for BAL quasars should be larger than that of unabsorbed quasars. If the difference between BALs and non-BALs is inclination (see, for example,

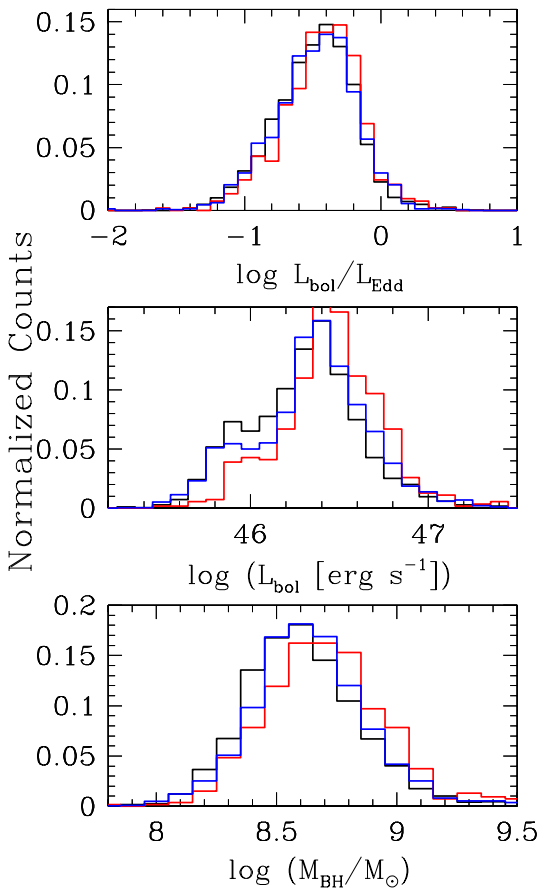


FIG. 4.— We compare the distribution of Eddington ratio (top), bolometric luminosity (middle), and black hole mass (bottom) between BAL QSOs (red or dark histogram), Unabsorbed QSOs (black or shaded histogram), and AAL QSOs (blue or light histogram). The distributions have been normalized to unit area.

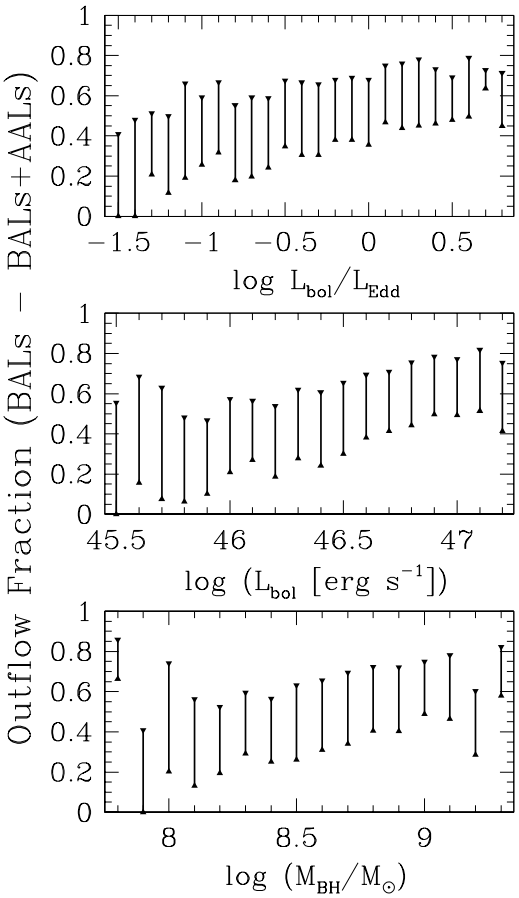


FIG. 5.— We show the fraction of quasars (relative to all quasars) with high-ionization outflows detected in C IV absorption as a function of Eddington ratio (top), bolometric luminosity (middle), and black hole mass (bottom). Lower limits arise from assuming that only the quasars in the mini-BAL/BAL sample are BALs, Upper limits arise from assuming that both mini-BAL/BAL and AAL quasar samples should be counted as outflows.

Brotherton et al. 2006, for a rebuttal of simple orientation schemes), then one might expect differences since how one views an axisymmetric object changes the spectrum one observes (e.g., Krolik & Voit 1998). Optical spectra of BAL do tend to be flatter than that of unabsorbed quasars (e.g., Yamamoto & Vansevičius 1999; Brotherton et al. 2001; Tolea et al. 2002; Reichard et al. 2003b, see also Figure 3). On the other hand, one might question the validity of the black hole mass scaling relations for BAL quasars, since they have been largely absent from reverberation mapping campaigns.[6] Inaccurate black hole masses would, of course, affect our computations of the Eddington luminosities.

In addition to the comparison in the mean values of the distributions, we also consider the BAL fraction as a function of various physical parameters. Figure 5 shows how the outflow fraction changes as a function of Eddington ratio, bolometric luminosity, and black hole mass. In each of the panels, we provide an upper limit and lower limit to the outflow fraction. The lower limit assumes that only quasars in our BAL sample should be counted as outflows:

$$\text{Outflow Frac.} \geq \frac{\text{BALs}}{\text{BALs} + \text{AALs} + \text{Unabsorbed}}. \quad (3)$$

However, it is still possible with our subjective classification scheme that some outflows (detected in absorption) were placed in the AAL class. Thus we place an upper limit on the fraction of quasars with detected outflows by assuming that all objects classified as BAL or AAL should be counted:

$$\text{Outflow Frac.} \leq \frac{\text{BALs} + \text{AALs}}{\text{BALs} + \text{AALs} + \text{Unabsorbed}}. \quad (4)$$

There are a number of possible origins for AALs (other than outflowing gas) so the incompleteness of the BAL sample is unlikely to be very large. Thus, the upper limit should be treated as a very conservative value.

Generally, there does seem to be a slight trend of increasing outflow fraction with increasing Eddington ratio, bolometric luminosity, and black hole mass. However, the distributions are, to within our conservative upper limits, consistent with being almost constant.

[6] To date, only one BAL quasar, PG 1700+518, has had a reported black hole mass from reverberation mapping (Vestergaard & Peterson 2006; Kaspi et al. 2005; Peterson et al. 2004; Kaspi et al. 2000).

Table 5. Sample Mean for Fitted and Derived Parameters

| Quantity | Unit | mini-BALs/BALs | AALs | Unabsorbed |
|---|---|---|---|---|
| $\langle \lambda L_\lambda(3000\,\text{Å})\rangle$ | $10^{45}$ erg s$^{-1}$ | 7.04±0.24 (5.67) | 5.88±0.14 (5.93) | 5.30±0.11 (5.48) |
| $\langle \alpha_{\rm NUV}\rangle$ | $F_\lambda \sim \lambda^{-\alpha}$ | 1.29±0.02 (0.45) | 1.50±0.01 (0.48) | 1.55±0.01 (0.42) |
| $\langle$Mg II FWHM$\rangle$ | $10^3$ km s$^{-1}$ | 4.94±0.06 (1.48) | 4.84±0.03 (1.33) | 4.75±0.03 (1.28) |
| $\langle L_{\rm bol}/L_{\rm Edd}\rangle$ | | 0.46±0.01 (0.33) | 0.41±0.01 (0.31) | 0.41±0.01 (0.32) |
| $\langle M_{\rm BH}\rangle$ | $10^8$ M$_\odot$ | 6.18±0.21 (4.95) | 5.16±0.09 (3.80) | 4.75±0.07 (3.32) |
| $\langle L_{\rm bol}\rangle$ | $10^{46}$ erg s$^{-1}$ | 3.52±0.12 (2.84) | 2.94±0.07 (2.96) | 2.65±0.05 (2.74) |

Note. — The mean values for each fitted property, continuum luminosity, spectra index, and Mg II $\lambda$2800 emission-line FWHM is reported for each quasar class. Parenthetical numbers indicate the standard deviations of the distributions.

Table 6. Spearman Rank Correlation Tests

| | BI | AI | $v_{\rm max}$ | $\langle v\rangle$ |
|---|---|---|---|---|
| $\lambda L_\lambda(3000\,\text{Å})$ | 0.047 / 0.286 | -0.018 / 0.684 | $\mathbf{0.264 / 7.5\times10^{-10}}$ | $\mathbf{0.200 / 3.7\times10^{-6}}$ |
| $\alpha_{\rm NUV}$ | 0.142 / 0.001 | 0.001 / 0.974 | $\mathbf{0.227 / 1.4\times10^{-7}}$ | $\mathbf{0.295 / 4.8\times10^{-12}}$ |
| Mg II FWHM | -0.113 / 0.010 | -0.069 / 0.113 | $\mathbf{-0.207 / 1.6\times10^{-6}}$ | $\mathbf{-0.194 / 7.5\times10^{-6}}$ |
| $M_{\rm BH}$ | -0.080 / 0.068 | -0.079 / 0.069 | -0.042 / 0.331 | -0.063 / 0.150 |
| $L_{\rm bol}/L_{\rm Edd}$ | 0.111 / 0.010 | 0.044 / 0.313 | $\mathbf{0.305 / 8.0\times10^{-13}}$ | $\mathbf{0.263 / 8.6\times10^{-10}}$ |
| | Width | Max. Depth | Num. Trough | |
| $\lambda L_\lambda(3000\,\text{Å})$ | 0.021 / 0.637 | $\mathbf{-0.282 / 4.8\times10^{-11}}$ | 0.142 / 0.001 | |
| $\alpha_{\rm NUV}$ | 0.058 / 0.186 | -0.125 / 0.004 | 0.004 / 0.920 | |
| Mg II FWHM | -0.055 / 0.208 | $1.7\times10^{-4}$ / 1.000 | -0.103 / 0.018 | |
| $M_{\rm BH}$ | -0.049 / 0.258 | $-0.160 / 2.3\times10^{-4}$ | -0.010 / 0.817 | |
| $L_{\rm bol}/L_{\rm Edd}$ | 0.051 / 0.241 | $-0.148 / 6.0\times10^{-4}$ | 0.140 / 0.001 | |

Note. — For each entry, we list the Spearman rank correlation statistic followed by the probability of the null hypothesis. The statistics for the bolometric luminosity are the same as those for $\lambda L_\lambda(3000\,\text{Å})$.

### 3.2. *Correlations With BAL Properties*

In Table 6 we report Spearman rank correlation statistics (and the corresponding probabilities of the null hypothesis) for correlations between the measured BAL properties from Trump et al. (2006, BI, AI, $v_{\rm max}$, $\langle v\rangle$, etc.) and our measured/derived quasar properties [$L_\lambda(3000\,\text{Å})$, $\alpha_{\rm NUV}$, $L_{\rm bol}/L_{\rm Edd}$, etc.]. In this correlation table, we have excluded the 11 BAL quasars that do not appear in the Trump et al. (2006) catalog. The BALnicity and absorption indices do not appear to be correlated with any of our measured/derived quasar properties. This is not surprising given these quantities, which are essentially variants of an equivalent width, are complicated functions that depend on the column density of the outflow, the covering factor of the flow, dilution by scattered light, and the overall kinematics of the flow.

The single quantity that appears to be correlated with most quasar properties is the maximum velocity of absorption. Highly significant (at least in terms of the Spearman rank statistics) correlations are found between $v_{\rm max}$ and the Eddington ratio and the 3000 Å luminosity. To a lesser extent, $v_{\rm max}$ also appears to be correlated with the NUV spectral index. Extreme values of $v_{\rm max}$ are purported to measure the terminal velocity of the mass outflow. In the current paradigm of radiatively-driven outflows (e.g., Arav et al. 1994; Murray et al. 1995; Laor & Brandt 2002), the significance of these correlations is not surprising. Naively, the number of photons (i.e., luminosity), distribution of momenta (i.e., the spectral shape), and black hole mass should play a role in determining the ability to drive an outflow. (Ionization of the gas will also play role, and we return to this issue later.) Oddly enough, there is not a significant correlation detected with black hole mass, but there is with Eddington ratio which incorporates the black hole mass.

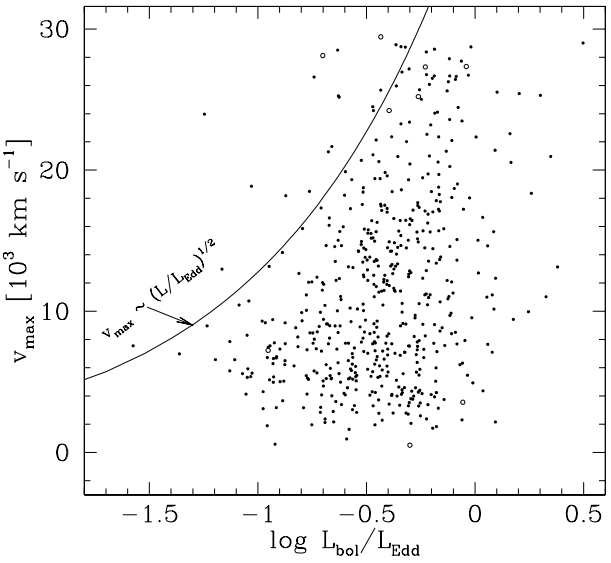


Fig. 6.— We show the correlation between the maximum velocity of absorption and the Eddington ratio. BAL quasars in the Trump et al. (2006) catalog are shown as filled circles. New BAL quasars from this work are shown as unfilled circles. The curve is a fiducial to show the predicted scaling relationship from Hamann (1998) and Misawa et al. (2007). The normalization of the curve is arbitrary.

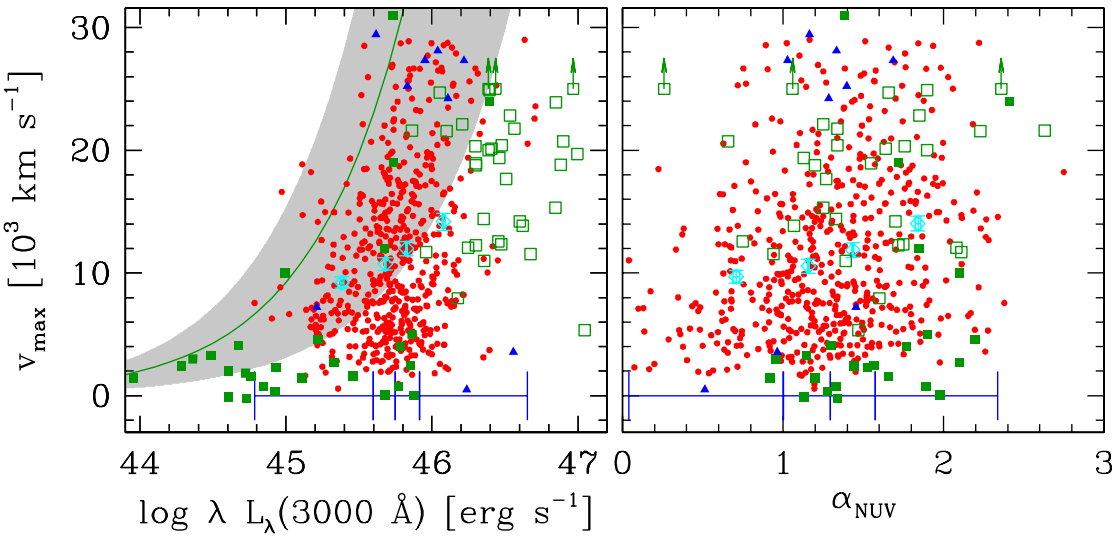


FIG. 7.— We show the correlation between the maximum velocity of absorption and 3000 Å luminosity (left) and near ultraviolet spectral index (right). BAL quasars in the Trump et al. (2006) catalog are shown as (red) circles. New BAL quasars from this work are shown as (blue) triangles. Filled (green) squares are the Palomar-Green quasars from Laor & Brandt (2002), while unfilled (green) squares are LBQS BAL quasars from Gallagher et al. (2006). Unfilled (cyan) diamonds indicate averages of $v_{max}$ and $L_\lambda(3000\,\text{Å})/\alpha_{NUV}$ for the Trump et al. (2006) BALs in bins that are indicated by the ticks on the (blue) horizontal line. The error bars on the points indicate the statistical uncertainties in the mean values. The bins were chosen to have equal numbers of objects (136). The green curve is the $v_{max}$-$L_\lambda(3000\,\text{Å})$ fit from Laor & Brandt (2002), while the shaded region indicates the reported $1\sigma$ uncertainty.

#### 3.2.1. $v_{max}$ *vs. Eddington Ratio*

Misawa et al. (2007) and Hamann (1998) show that the terminal velocity of the outflow should scale with the Eddington ratio [$v_{terminal} \sim (L_{bol}/L_{Edd})^{1/2}$]. In Figure 6, we plot $v_{max}$ against the our derived Eddington ratio for our BAL quasars sample (BAL quasars in the Trump et al. (2006) sample are shown as filled symbols, while the additional 11 BAL quasars are shown with unfilled symbols). We show a fiducial curve with the predicted scaling and an arbitrary normalization. Overall, there does appear to be an upper envelope that seems to scale as predicted. An actual empirical fit to the envelope would probably favor a steeper (i.e., larger exponent) scaling.

We note one BAL quasar that appears largely discrepant with the apparent envelope, SDSS J145408.25+045053.54 ($z_{em} = 1.98127$). We derived an Eddington ratio of $\log L_{bol}/L_{Edd} \approx -1.25$. In addition to the clear broad C IV absorption-line, Trump et al. (2006) detect a narrow C IV absorption-line system ($v_{FWHM} \lesssim 500\,\text{km s}^{-1}$) at $z_{abs} = 1.7654$, and report a maximum velocity of absorption $v_{max} = 23184\,\text{km s}^{-1}$. However, in addition to being narrow, this system also shows absorption in a plethora of low-ionization species (Al II-III, Mg II, Si II, Si IV, Fe II) and, arguably, should not be counted as intrinsic absorption. If this system is discounted, then $v_{max}$ for this BAL quasar would be closer to $14000\,\text{km s}^{-1}$, which is more consistent with the apparent envelope of the other BAL quasars.

#### 3.2.2. $v_{max}$ *vs. Luminosity and Spectral Index*

In addition to the Eddington ratio, the maximum velocity of absorption also appears to be correlated with the 3000 Å luminosity and the NUV spectral index. Figure 7 shows plots of $v_{max}$ against these latter two quantities. In both panels we distinguish between SDSS BAL quasars that appear in the Trump et al. (2006) catalog (plotted as red filled circles) and the 11 new BAL quasars that we added from our subjective search (plotted as blue filled triangles). In addition, we have plotted the BAL quasars from the Bright Quasar Survey as tabulated by Laor & Brandt (2002, green filled squares), and from the Large Bright Quasar Survey as tabulated by Gallagher et al. (2006, green open squares.).

In the $v_{max} - L_\lambda(3000\,\text{Å})$ panel, we also reproduce the fit (corrected for our cosmology) to the soft X-ray weak PG quasars carried out by Laor & Brandt (2002). For the updated fit, we have used the same quasars as Laor & Brandt (2002). We note two differences in our approach from the Laor & Brandt (2002) approach. First, Laor & Brandt (2002) fit all soft X-ray weak quasars in the PG catalog. Soft X-ray weak quasars are defined as those having $\alpha_{ox} \leq -2$, where $\alpha_{ox}$ is the spectral index derived from the flux at 2500 Å and 2 keV. BALs are a subset of soft X-ray weak quasars. Laor & Brandt (2002) noted that soft X-ray weak quasars appeared to define an upper envelope to the $v_{max} - L_\lambda(3000\,\text{Å})$ plot, consistent with the idea that the absorption does not always trace the terminal velocity of the outflow. We note here (and discuss further in §4) that, with the inclusion of the SDSS BALs, it is clear that there is indeed an envelope (though BALs by themselves do not define it), and our fit should reflect that. Consequently, we have excluded PG 2112+059 from the fit since it clearly does not trace the envelope of the plot (see Figure 7, left panel where it is plotted at $\lambda L_\lambda(3000\,\text{Å}) \sim 10^{46.2}\,\text{erg s}^{-1}$ and $v_{max} \sim 24000\,\text{km s}^{-1}$). There a number of BALs at smaller luminosities that have larger $v_{max}$ values. Fur-

thermore, there are LBQS BALs at comparable luminosities that show larger $v_{\rm max}$ values. In carrying out the new fit *of the envelope*, we have assumed a 10% uncertainty in both velocity and luminosity. The parameters of the revised fit are:

$$v = v_{\rm o}(L/L_{\rm o})^{\alpha}, \quad (5)$$
$$\log L_{\rm o}({\rm erg\ s^{-1}}) = 45.0,$$
$$\alpha = 0.662 \pm 0.004,$$
$$\log v_{\rm o}({\rm km\ s^{-1}}) = 3.96 \pm 0.29.$$

We have chosen to exclude the SDSS BAL quasars from the fit because we do not have a convenient criterion for selecting which quasars define the upper envelope. Laor & Brandt (2002) fit all soft X-ray weak quasars (defined at those having $\alpha_{\rm ox} \leq -2$), since these appeared to define their envelope. This criterion would not work here for a few reasons:

1. Since our quasars lie in the redshift range 1.7–2.0, most of our quasars are not detected in, for example, the *ROSAT* All-Sky Survey. So we do not have a convenient way of computing $\alpha_{\rm ox}$ *en masse* for all of our BAL quasars.

2. Strateva et al. (2005) and Steffen et al. (2006) have quantified the dependence of $\alpha_{\rm ox}$ on luminosity [$\alpha_{\rm ox} = -0.136 \log L_{\nu}(2500\,{\rm \AA}) + 2.630$]. Consequently, it is possible that soft X-ray weakness as defined by $\alpha_{\rm ox}$ is not a reasonable criterion for defining the envelope. From the equation, the range in our luminosities ($\sim$2 dex) implies a scatter in the intrinsic (i.e., unabsorbed) value of $\alpha_{\rm ox}$ of $\sigma_{\alpha_{\rm ox}} \sim 0.27$.

3. Since all of our objects are pre-selected to have BAL troughs (even though the maximum observed velocities may be small), is it possible that all objects may be absorbed in the soft X-ray, and therefore would be included in the fit if a $\alpha_{\rm ox}$ criterion were used. This depends on the detailed relationship between soft X-ray absorption and UV BALs. See, for example, Gallagher et al. (2006) for a discussion of this.

There is a lot of scatter in each of the panels. So, to bring out the highly significant correlation, we have taken averages of all three quantities in four bins. The bins are chosen to have the same number of points (136) and so they are equally statistically significant and independent. The error bars indicate the statistical uncertainties in the mean values.

For the most part, if we interpret our revised $v_{\rm max} - L_{\lambda}(3000\,{\rm \AA})$ fit to the Laor & Brandt (2002) data as an upper envelope, the SDSS BAL quasars are very consistent with it, and fill in the entire range of velocities over the sampled luminosity range (which overlaps both the BQS and LBQS samples). Of the 536 BALs, only 2 BAL lies more than $1\sigma$ above the curve, and 11 BALs are more deviant than PG 1700+518, or PG 1001+054 which were used in reproducing the Laor & Brandt (2002) fit.

Another BAL parameter that appears to be correlated with one of the quasar physical parameters is the maximum depth of the profile (with both monochromatic and bolometric luminosities). We will examine the implications of this and correlations between BAL properties (which is important for interpreting this apparent correlation) in a future work.

## 4. DISCUSSION

### 4.1. *Are BALs Super-Accretors?*

From the comparison of Eddington ratios between BALs and unabsorbed quasars, we are led to conclude that BAL quasars are not super-accretors. While some fraction of BALs appear to accrete near or above the Eddington limit (51/536 with $L_{\rm bol}/L_{\rm Edd} \geq 0.8$), there are a significant number of BAL quasars that accrete at markedly sub-Eddington rates (358/536 with $L_{\rm bol}/L_{\rm Edd} \leq 0.5$). $L_{\rm bol}/L_{\rm Edd} \sim 0.5$ may not be considered a particularly "low" rate, especially in comparison with lower-luminosity AGN. However, it is important to note that BALs do not segregate themselves from other AGN in their distribution of Eddington ratios (Fig. 4) and the fraction of quasars with BALs remains significant down to "low" Eddington ratios ($\sim 0.03$, Fig.5).

While Fig. 5 apparently shows a BAL fraction of $\sim$0 at lower Eddington ratios, this is only an artifact of small number statistics. We only have six quasars in our sample with $L_{\rm bol}/L_{\rm Edd} \leq 0.03$, and one is a BAL, giving a BAL fraction of 16.7%. Moreover, very low luminosity quasars may not be capable of driving an outflow with a large velocity dispersion, but may still have significant outflows. We note that four of the six $L_{\rm bol}/L_{\rm Edd} \leq 0.03$ quasars do show AALs.

This is somewhat puzzling given that supposedly BAL quasars lie at one extreme of the Boroson & Green (1992) Eigenvectors 1 and 2 (Boroson & Green 1992; Yuan & Wills 2003). Boroson (2002) interpreted the Eddington ratio and the absolute mass accretion rate as the principal drivers of these two eigenvectors (see their Figure 7 which provides an interpretive diagram). BAL quasars are thought to occupy the high $L_{\rm bol}/L_{\rm Edd}$-high $\dot{M}_{\rm acc}$ region of this diagram. Our result apparently contradicts this idea.

There are two issues here in understanding why the Boroson (2002) interpretation may be too simple: (1) the BALs in the Boroson sample may not sample the full range of Eigenvector 1 properties allowed by the BAL parent population, and (2) the interpretation of Eddington ratio as the principal driver of Eigenvector 1 may not be correct (or complete).

There are only $\sim$ 4 BALs in the sample of 162 objects employed in the Boroson analysis. Thus, it is possible that these four objects simply do not sample the full range of Eigenvectors 1 and 2 that is allowed by the parent population of BAL quasars. (In comparison, we have increased the sample by more than a couple orders of magnitude.) On the other hand, from an analysis of 11 $z \sim 2$ BAL quasars, Yuan & Wills (2003) find that they do seem to lie on one extreme of the Fe II – [O III] distribution. Since this correlation is one of primary constituents of Eigenvector 1, they conclude that $z \sim 2$ BAL quasars lie at one extreme of Eigenvector 1 like their low-z kin. We note, however, that another ingredient of Eigenvector 1 is the H$\beta$ FWHM. From Figure 2 of Yuan & Wills (2003), it appears that the range of H$\beta$ FWHM for BAL quasars overlaps completely with that of non-BAL quasars, so this assertion is not strictly true. BAL quasars at higher redshift are not simply extreme

Eigenvector 1 objects.

We note that all objects in the Boroson (2002) sample lie at low redshift ($z \lesssim 0.8$), while all of our objects lie at higher redshift ($1.7 \lesssim z \lesssim 2$). It is possible that there is some form of evolution in the population of BAL quasars (e.g., luminosity changes or differences in black hole mass) such that low redshift objects have systematically high Eddington ratios while higher redshift BAL quasars do not. It is also possible the first principal component of quasar optical properties changes with redshift. Our result is further supported by Yuan & Wills (2003), who find $z \sim 2$ BAL quasars with Eddington ratios as low as $\sim 0.17$. This implies that accretion rate is not the principal driver of Eigenvector 1 properties (or that it is a secondary effect that is true only at low-z).

Yuan & Wills (2003) speculate that the principal driver of Eigenvector 1 may instead be the availability of "cold" gas fueling the accretion disk as implied, perhaps, by the strong Fe II and weaker [O III] emission. In this interpretation, the high correlation between Eigenvector 1 and the Eddington ratio in low redshift PG sample is seen as a secondary correlation. At low redshift, most objects have a low fuel supply, hence low Eddington ratio, and the few that have an abundance of cold fuel are able to accrete near the Eddington rate. These low redshift, high Eddington ratio black holes, are those that can exhibit broad absorption lines. At high redshift, however, most quasars (i.e., both BAL and non-BAL quasars) have an ample supply of cold gas with BAL quasars having the largest supply (perhaps because they are the youngest sources). Consequently, all high redshift quasars are able to accrete near their Eddington limits, hence having similar (and "high") Eddington ratios. Those that have the largest supply of cold gas, and hence largest fueling rates, have the largest outflow rate and exhibit broad absorption lines.

We note that an important component of the Yuan & Wills (2003) interpretation is the differences in black hole mass between their high redshift sample and the low redshift PG sample. The high redshift quasars from Yuan & Wills (2003) have masses $\gtrsim 10^9\,M_\odot$, whereas the low redshift PG quasars have lower masses ($< 10^9\,M_\odot$). It is this fact that allows the the high redshift quasars to accommodate higher absolute accretion rates (since they have larger Eddington accretion rates) and have higher luminosities than the low redshift PG quasars.

Our sample of quasars from SDSS is at similar redshifts to those in the Yuan & Wills (2003) sample ($z \sim 2$), but have smaller black hole masses, smaller bolometric luminosities and span a wider range of Eddington ratios. Compared to the low redshift PG sample, however, we have larger black hole masses, larger bolometric luminosities, but comparable range of Eddington ratios. Since we do not have rest-frame optical spectra for these quasar, their Eigenvector 1 properties are not known directly. Further study (e.g., infrared spectroscopy) is needed to understand how the Eigenvector 1 properties of these objects relate to the low redshift PG sample and the high redshift Yuan & Wills (2003) sample.

Nevertheless, if we take at face value the fact that we see BAL quasars in 16.7% (and outflows in as many as 83%) of $L_{\rm bol}/L_{\rm Edd} \leq 0.03$ objects, then we must question the completeness of the Yuan & Wills (2003) interpretation. High redshift BAL and non-BAL quasars do have similar Eddington ratios, but not because both populations are accreting near their Eddington limits. Even if we accept that BAL quasars do indeed lie at one extreme of the [O III] $\lambda$5007 equivalent width - Fe II/H$\beta$ intensity ratio anti-correlation, we must understand first the detailed physics governing that anti-correlation and drivers behind it. Yuan & Wills (2003) have shown that it is not simply the Eddington ratio. The addition of this work questions if it is simply the fueling rate. There are other effects, such as the covering factor of the outflow and underlying cause(s) of that covering factor, that must be considered in this interpretation.

### 4.2. *Radiatively-driven winds?*

Our second result is a confirmation of the luminosity-dependent envelope to the maximum velocity of absorption (Laor & Brandt 2002). From Figure 7, the maximum velocities of our BAL quasars appear to obey the $v \sim L^{0.66}$ best-fit relation re-derived with the corrected cosmology. To explain the slope, those authors consider two formulations of terminal velocity and its dependence on luminosity: $v_{\rm max} \propto \sqrt{\Gamma L/R}$, where $L$ is the luminosity, $R$ is the launching radius of the wind, and $\Gamma$ is the force-multiplier (Castor et al. 1975). Aside from the explicit $\sqrt{L}$ factor, the luminosity also comes into play in determining both the force-multiplier and the launching radius. One can assume that the launching radius is independent of luminosity or that there is a scaling (e.g., $R \sim \sqrt{L}$). This gives a range of velocity scalings: $v_{\rm max} \sim \sqrt{\Gamma} L^{0.25-0.5}$. The original Laor & Brandt (2002) best fit had a steeper slope which led the authors to conclude that there was a luminosity dependence to the force-multiplier. We agree with that conclusion with a cosmology-corrected revision of the required dependence (combining the theoretical dependence of $v_{\rm max}$ on $\Gamma$ and luminosity with our revised best-fit to the $v_{\rm max} - L_\lambda(3000\,\text{Å})$ envelope): $\Gamma \sim L^{0.32-0.82}$.

The force multiplier, $\Gamma$, relates the force from a line-driven (or edge-driven) wind to one that is driven purely by electron (Thompson) scattering. UV transitions (e.g., in the range 200-3200 Å) are thought to be principal contributors to line-driving. The precise relationship between the force multiplier and the luminosity (or, alternatively, ionization parameter) can be complicated (e.g., Arav et al. 1994), and is beyond the scope of this paper. It is sufficient here to say that a relationship between the force-multiplier and the luminosity is expected (i.e., the two quantities are not *a priori* expected to be independent).

Sulentic et al. (2006) employ the semi-empirical $\Gamma(U)$ relationship derived by Arav & Li (1994, $\log\Gamma \approx 2.551 - 0.536\log U$) to explicitly characterize the dependence of $v_{\rm max}$ with ionization parameter ($v_{\rm max} \sim U^{-1/4}$). We clarify here that this relationship is only valid under certain conditions which are not necessarily valid throughout a BAL flow: (1) the relationship does not account for optical depth effects[7] (all lines are assumed to be highly optically thin), (2) the force multiplier only takes into account line-driving (driving from edges may also

[7] The full relation given in Arav & Li (1994) does include terms accounting for optical depth, but these were not included in the Sulentic et al. (2006) analysis.

be important), (3) the driving spectrum is that derived by Mathews & Ferland (1987) which may not be generally applicable, and (4) the range of valid ionization parameters is small ($-1.5 \leq \log U \leq +0.5$). A revision of this relation given in Arav, Li, & Begelman (1994) expanded the range of ionization parameter to $-3 \leq \log U \leq 1$, but with a more complicated semi-empirical fit: $\log \Gamma = 3.642 - 0.1445[\log U + 3]^2$. [Note that this still uses the Mathews & Ferland (1987) spectrum and also does not account for optical depth effects.] Furthermore, Proga et al. (1998) and Proga & Kallman (2004) note that the force-multiplier is very sensitive to both the Eddington ratio and to the black hole mass. A line-driven wind cannot be formed unless $L_{\rm bol}/L_{\rm Edd} \gtrsim \Gamma^{-1}$.

Another complication in the evaluation of the force-multiplier (as we have noted) and its effect on the terminal velocity of the wind is the dependence on the shape of the driving spectrum. From our fits, we have a hint of this importance in the apparent correlation between $v_{\rm max}$ and $\alpha_{\rm NUV}$. The correlation (Fig. 7, right panel) is weak, but statistically significant (Table 6). The only resonant lines in the NUV region of the spectrum are Mg II$\lambda\lambda$2796,2803 and the plethora of Fe II lines in the range 2230–2600 Å. In the high-ionization BALs in this analysis, it is unlikely the these transitions play an important role in line-driving. A more likely cause for the correlation is the loose dependence between $\alpha_{\rm NUV}$ and the UV flux at shorter wavelengths, in the sense that "harder" values of $\alpha_{\rm NUV}$ will yield relatively more UV/FUV photons than "softer" values. [Note that, with our sign convention, $F_\lambda \sim \lambda^{-\alpha}$, a larger value of $\alpha_{\rm NUV}$ implies a harder spectrum.] We note here that, in our sample, $\alpha_{\rm NUV}$ is anti-correlated with $L_\lambda(3000\,\text{Å})$ (i.e., more luminous sources are "softer"). Thus the correlation between $v_{\rm max}$ and $L_\lambda(3000\,\text{Å})$ contributes to the weakness in the correlation between $v_{\rm max}$ and $\alpha_{\rm NUV}$. Consequently, the dependence of $v_{\rm max}$ on $\alpha_{\rm NUV}$ is probably stronger than indicated.

Finally, we note that $v_{\rm max}$ - $\lambda L_\lambda(3000\,\text{Å})$ curve truly constitutes an upper envelope. A significant fraction of points lie well below the curve. The details in the computation of the force-multiplier likely can explain some of this. However, there are a few other possibilities to note. As with all objects that do not show spherical symmetry, the orientation relative to the observer's sight-line probably plays a role. The magnitude of this effect is not clear, and is affected by the fact that we do not yet have a full theoretical exploration of the accretion disk-wind paradigm. [For example, the orientation of radio-jets and polarization of light in the troughs in some radio-loud BALs seems to indicate a range of accretion-disk orientations (Zhou et al. 2006; Brotherton et al. 2006), but the opening angle of the wind may also be important.] Moreover, while the existence of the $v_{\rm max}$ - $\lambda L_\lambda(3000\,\text{Å})$ envelope indicates the importance of radiation-pressure in driving the BAL outflow, this is not the only possible mechanism. Magnetically-driven (e.g., Everett 2005), and thermally-driven (e.g., Krolik & Kriss 2001) winds may explain some fraction of BALs with smaller observed values of $v_{\rm max}$.

For the Laor & Brandt (2002) points that appear at low $v_{\rm max}$, one must also question the location of the absorbing gas. It is possible that some of these may be unrelated to the immediate quasar environment, and may arise from the ISM of the host galaxy, or perhaps other nearby galaxies. However, this cannot explain the objects from our sample that have small $v_{\rm max}$. As we noted before, all of our objects are selected because they show broad wind-like profiles. Absorption from the host galaxy or nearby structures would have velocity dispersions of a few hundred km s$^{-1}$ appearing close to the quasar redshift, and thus would have been relegated to our AAL class. The low-velocity objects in our sample may indicate the importance of non-radiative processes like thermal gradients (e.g., Krolik & Kriss 2001) or magneto-centrifugal rotation (e.g., Everett 2005) in driving outflows.

A further complication is the apparently redshifted absorption that we have in some of our BALs. In the case of host galaxy ISM absorption, this would not be a problem since the C IV $\lambda$1549 emission line is known to be blueshifted with respect to the systemic redshift (e.g., Gaskell 1983; Espey 1993; Richards et al. 2002; Vanden Berk et al. 2001). However, in the accretion-disk/wind paradigm, the C IV broad emission and broad absorption lines are thought to be produced by different parts of the same flow (Murray et al. 1995; Baldwin et al. 1996; Murray & Chiang 1997; Elvis 2000). [Some fraction of the C IV $\lambda$1549 emission line may arise from different regions, like a virialized component (e.g., Wills et al. 1993; Brotherton et al. 1994), but seems to be dominated by a wind component.] A full interpretation of how (or whether) this situation (apparently redshifted broad absorption sitting on top of a blueshifted broad emission line) is complicated by the uncertainty in what part or parts of the wind are being sampled by the observed absorption and in what determines the velocity where the emissivity peaks. Both of these questions rely on the orientations of the observer relative to the axis of the disk and to the direction (and opening angle) of the wind, as well as the dynamics and ionization structure of the wind.

## 5. SUMMARY

1. We have subjectively scrutinized a sample of 5088 $1.7 \leq z \leq 2$ quasars from the Second Data Release of the Sloan Digital Sky Survey and placed the objects into three classes: 562 objects show clear signs of an outflow; 2573 show no signs of an outflow (in absorption); 1898 show evidence of "associated" narrow absorption which could have several different locations. The frequency of observed outflows is different from the recent AI-based BAL catalog of Trump et al. (2006) and we point out several differences.

2. We have estimated black hole masses and Eddington ratios for all quasars in this sample. We find that there is no appreciable difference in either the black hole mass or Eddington ratio distribution between BALs and non-BALs. This implies that BALs in this redshift range are not super-accretors. Like Yuan & Wills (2003), we speculate that Eddington ratio may not be the principal driver of the Boroson & Green (1992) Eigenvector 1, but rather availability of cold gas, and the "down-sizing" evolution of black-hole mass in accreting systems.

3. We find that the maximum velocity of absorption as a function of luminosity has an upper envelope that is consistent with the best fit from Laor & Brandt (2002). This upper envelope is easily interpreted as the terminal velocity of radiatively-driven wind. We find that it is also correlated with NUV spectral index, which may indicate the importance of the SED shape in governing the dynamics of the outflow. However, many of our BALs terminate at small velocities. This may indicate the importance of wind-orientation, or non-radiative processes in driving outflows.

We wish to thank Sarah Gallagher, Toru Misawa, Ari Laor, Jonathan Trump, Gordon Richards, and John Everett for helpful discussions. Special thanks are given to the referee Pat Hall for an excellent, thorough, and well-thought out review of the paper. This work was supported by the National Science Foundation under Grant No. 0507781.

Funding for the SDSS and SDSS-II has been provided by the Alfred P. Sloan Foundation, the Participating Institutions, the National Science Foundation, the U.S. Department of Energy, the National Aeronautics and Space Administration, the Japanese Monbukagakusho, the Max Planck Society, and the Higher Education Funding Council for England. The SDSS Web Site is http://www.sdss.org/.

The SDSS is managed by the Astrophysical Research Consortium for the Participating Institutions. The Participating Institutions are the American Museum of Natural History, Astrophysical Institute Potsdam, University of Basel, University of Cambridge, Case Western Reserve University, University of Chicago, Drexel University, Fermilab, the Institute for Advanced Study, the Japan Participation Group, Johns Hopkins University, the Joint Institute for Nuclear Astrophysics, the Kavli Institute for Particle Astrophysics and Cosmology, the Korean Scientist Group, the Chinese Academy of Sciences (LAMOST), Los Alamos National Laboratory, the Max-Planck-Institute for Astronomy (MPIA), the Max-Planck-Institute for Astrophysics (MPA), New Mexico State University, Ohio State University, University of Pittsburgh, University of Portsmouth, Princeton University, the United States Naval Observatory, and the University of Washington.

REFERENCES

Abazajian, K., et al. 2004, AJ, 128, 502
Arav, N., & Li, Z.-Y. 1994, ApJ, 427, 700
Arav, N., Li, Z.-Y., & Begelman, M. C. 1994, ApJ, 432, 62
Baldwin, J. A., et al. 1996, ApJ, 461, 664
Becker, R. H., White, R. L., Gregg, M. D., Brotherton, M. S., Laurent-Muehleisen, S. A., & Arav, N. 2000, ApJ, 538, 72
Boroson, T. A. 2002, ApJ, 565, 78
Boroson, T. A., & Green, R. F. 1992, ApJS, 80, 109
Brandt, W. N., & Gallagher, S. C. 2000, New Astronomy Review, 44, 461
Brotherton, M. S., de Breuck, C., & Schaefer, J. J. 2006, MNRAS, 372, L58
Brotherton, M. S., Tran, H. D., Becker, R. H., Gregg, M. D., Laurent-Muehleisen, S. A., & White, R. L. 2001, ApJ, 546, 775
Brotherton, M. S., et al. 1999, ApJ, 520, L87
Brotherton, M. S., Wills, B. J., Steidel, C. C., & Sargent, W. L. W. 1994, ApJ, 423, 131
Castor, J. I., Abbott, D. C., & Klein, R. I. 1975, ApJ, 195, 157
Dietrich, M., & Hamann, F. 2004, ApJ, 611, 761
Elvis, M. 2000, ApJ, 545, 63
Espey, B. R. 1993, ApJ, 411, L59
Everett, J. E. 2005, ApJ, 631, 689
Gallagher, S. C., Brandt, W. N., Chartas, G., Priddey, R., Garmire, G. P., & Sambruna, R. M. 2006, ApJ, 644, 709
Gallagher, S. C., Brandt, W. N., Sambruna, R. M., Mathur, S., & Yamasaki, N. 1999, ApJ, 519, 549
Gaskell, C. M. 1983, ApJ, 267, L1
Goodrich, R. W. 1997, ApJ, 474, 606
Goodrich, R. W., & Miller, J. S. 1995, ApJ, 448, L73
Gregg, M. D., Becker, R. H., Brotherton, M. S., Laurent-Muehleisen, S. A., Lacy, M., & White, R. L. 2000, ApJ, 544, 142
Gregg, M. D., Becker, R. H., & de Vries, W. 2006, ApJ, 641, 210
Hall, P. B., et al. 2002, ApJS, 141, 267
Hamann, F. 1998, ApJ, 500, 798
Kaspi, S., Maoz, D., Netzer, H., Peterson, B. M., Vestergaard, M., & Jannuzi, B. T. 2005, ApJ, 629, 61
Kaspi, S., Smith, P. S., Netzer, H., Maoz, D., Jannuzi, B. T., & Giveon, U. 2000, ApJ, 533, 631
Kriss, G. 1994, in ASP Conf. Ser. 61: Astronomical Data Analysis Software and Systems III, ed. D. R. Crabtree, R. J. Hanisch, & J. Barnes, 437
Krolik, J. H. 1999, Active Galactic Nuclei : From The Central Black Hole To The Galactic Environment (Princeton, N. J. : Princeton University Press, c1999.)
Krolik, J. H., & Kriss, G. A. 2001, ApJ, 561, 684
Krolik, J. H., & Voit, G. M. 1998, ApJ, 497, L5
Laor, A., & Brandt, W. N. 2002, ApJ, 569, 641
Mathews, W. G., & Ferland, G. J. 1987, ApJ, 323, 456
McLure, R. J., & Jarvis, M. J. 2002, MNRAS, 337, 109
Misawa, T., Charlton, J. C., Eracleous, M., Ganguly, R., Tytler, D., Kirkman, D., Suzuki, N., & Lubin, D. 2007, ApJ, in press (astro-ph/0702101)
Murray, N., & Chiang, J. 1997, ApJ, 474, 91
Murray, N., Chiang, J., Grossman, S. A., & Voit, G. M. 1995, ApJ, 451, 498
Najita, J., Dey, A., & Brotherton, M. 2000, AJ, 120, 2859
Peterson, B. M., et al. 2004, ApJ, 613, 682
Proga, D., & Kallman, T. R. 2004, ApJ, 616, 688
Proga, D., Stone, J. M., & Drew, J. E. 1998, MNRAS, 295, 595
Reichard, T. A., et al. 2003a, AJ, 126, 2594
Reichard, T. A., et al. 2003b, AJ, 125, 1711
Richards, G. T., et al. 2003, AJ, 126, 1131
Richards, G. T., et al. 2006, ApJS, 166, 470
Richards, G. T., Vanden Berk, D. E., Reichard, T. A., Hall, P. B., Schneider, D. P., SubbaRao, M., Thakar, A. R., & York, D. G. 2002, AJ, 124, 1
Sanders, D. B., Soifer, B. T., Elias, J. H., Neugebauer, G., & Matthews, K. 1988, ApJ, 328, L35
Shang, Z., et al. 2005, ApJ, 619, 41
Sprayberry, D., & Foltz, C. B. 1992, ApJ, 390, 39
Steffen, A. T., Strateva, I., Brandt, W. N., Alexander, D. M., Koekemoer, A. M., Lehmer, B. D., Schneider, D. P., & Vignali, C. 2006, AJ, 131, 2826
Strateva, I. V., Brandt, W. N., Schneider, D. P., Vanden Berk, D. G., & Vignali, C. 2005, AJ, 130, 387
Sulentic, J. W., Dultzin-Hacyan, D., Marziani, P., Bongardo, C., Braito, V., Calvani, M., & Zamanov, R. 2006, Revista Mexicana de Astronomia y Astrofisica, 42, 23
Tolea, A., Krolik, J. H., & Tsvetanov, Z. 2002, ApJ, 578, L31
Trump, J. R., et al. 2006, ApJS, 165, 1
Vanden Berk, D. E., et al. 2001, AJ, 122, 549
Vestergaard, M. 2004, ApJ, 601, 676
Vestergaard, M., & Peterson, B. M. 2006, ApJ, 641, 689
Vestergaard, M., & Wilkes, B. J. 2001, ApJS, 134, 1
Voit, G. M., Weymann, R. J., & Korista, K. T. 1993, ApJ, 413, 95
Weymann, R. J., Morris, S. L., Foltz, C. B., & Hewett, P. C. 1991, ApJ, 373, 23
Wills, B. J., Brotherton, M. S., Fang, D., Steidel, C. C., & Sargent, W. L. W. 1993, ApJ, 415, 563
Wise, J. H., Eracleous, M., Charlton, J. C., & Ganguly, R. 2004, ApJ, 613, 129

Table 7. Measured and Derived Quasar Parameters

| Name | MJD | Plate | Fiber | Redshift | $F_\lambda$ | $\alpha_{\rm NUV}$ | $\lambda L_\lambda$ | Mg II FWHM | $M_{\rm BH}$ | $L_{\rm bol}/L_{\rm Edd}$ | Run | Class |
|---|---|---|---|---|---|---|---|---|---|---|---|---|
| SDSS J000009.42 − 102751.88 | 52143 | 0650 | 199 | 1.844230 | 2.2672 | 1.802 | 4.577 | 12320 | 30.856 | 0.0491 | 2 | AAL |
| SDSS J000058.24 − 004646.29 | 51791 | 0387 | 093 | 1.895120 | 2.9567 | 1.763 | 6.496 | 4560 | 4.983 | 0.4316 | 1 | Reg |
| SDSS J000118.42 − 010221.60 | 51791 | 0387 | 042 | 1.968500 | 1.2266 | 1.843 | 3.033 | 9200 | 14.180 | 0.0708 | 3 | AAL |
| SDSS J000119.64 + 154828.78 | 52235 | 0750 | 566 | 1.924210 | 2.3214 | 1.301 | 5.347 | 4885 | 5.219 | 0.3393 | 3 | BAL |
| SDSS J000139.43 + 152624.11 | 52235 | 0750 | 541 | 1.789660 | 5.8318 | 1.246 | 10.727 | 4370 | 5.793 | 0.6131 | 1 | Reg |
| SDSS J000139.64 − 103824.05 | 52143 | 0650 | 136 | 1.820630 | 1.9547 | 1.017 | 3.792 | 4300 | 3.441 | 0.3649 | 2 | Reg |
| SDSS J000219.34 − 105259.58 | 52143 | 0650 | 097 | 1.762000 | 0.9092 | 0.436 | 1.594 | 5245 | 3.406 | 0.1549 | 2 | AAL |
| SDSS J000221.80 + 151454.59 | 52235 | 0750 | 553 | 1.823530 | 3.3027 | 1.123 | 6.438 | 3840 | 3.519 | 0.6058 | 3 | AAL |
| SDSS J000319.87 − 090156.19 | 52143 | 0650 | 561 | 1.760220 | 9.9334 | 1.637 | 17.356 | 3390 | 4.371 | 1.3148 | 3 | Reg |
| SDSS J000422.30 − 090219.36 | 52143 | 0650 | 609 | 1.858810 | 5.1395 | 1.323 | 10.633 | 3370 | 3.431 | 1.0262 | 2 | Reg |
| SDSS J000510.84 − 092534.79 | 52143 | 0650 | 621 | 1.866540 | 1.6132 | 1.170 | 3.381 | 3635 | 2.330 | 0.4805 | 3 | Reg |
| SDSS J000546.49 − 002413.98 | 51793 | 0388 | 268 | 1.729750 | 2.0840 | 1.133 | 3.450 | 3705 | 2.443 | 0.4675 | 3 | Reg |
| SDSS J000612.30 − 104310.65 | 52141 | 0651 | 258 | 1.735310 | 3.3973 | 1.481 | 5.680 | 3455 | 2.686 | 0.7003 | 2 | Reg |
| SDSS J000629.29 − 093550.93 | 52141 | 0651 | 429 | 1.758180 | 5.0479 | 0.936 | 8.788 | 6880 | 13.075 | 0.2226 | 2 | Reg |
| SDSS J000648.74 − 094037.00 | 52141 | 0651 | 468 | 1.835040 | 2.5152 | 0.686 | 5.000 | 3970 | 3.340 | 0.4957 | 2 | AAL |
| SDSS J000654.11 − 001533.30 | 51793 | 0388 | 234 | 1.725170 | 7.5664 | 0.943 | 12.422 | 4650 | 7.028 | 0.5853 | 4 | Reg |
| SDSS J000735.52 − 085435.16 | 52141 | 0651 | 417 | 1.777750 | 2.4386 | 1.561 | 4.394 | 3315 | 2.191 | 0.6639 | 2 | Reg |
| SDSS J000759.40 + 150822.65 | 52251 | 0751 | 557 | 1.968020 | 2.4355 | 0.887 | 6.017 | 2915 | 1.964 | 1.0143 | 2 | Reg |
| SDSS J000815.33 − 095854.03 | 52141 | 0651 | 494 | 1.949790 | 6.6211 | 0.854 | 15.891 | 4420 | 7.129 | 0.7381 | 1 | AAL |
| SDSS J000904.43 − 004332.85 | 51793 | 0388 | 098 | 1.828630 | 3.8336 | 1.089 | 7.538 | 3700 | 3.518 | 0.7094 | 4 | Reg |
| SDSS J000919.26 + 152355.17 | 52251 | 0752 | 343 | 1.934950 | 1.4671 | 1.883 | 3.439 | 4730 | 3.976 | 0.2864 | 2 | AAL |
| SDSS J001017.52 − 100238.90 | 52138 | 0652 | 316 | 1.819020 | 2.8847 | 1.216 | 5.581 | 4075 | 3.705 | 0.4987 | 2 | AAL |
| SDSS J001017.81 + 010450.74 | 51793 | 0388 | 607 | 1.817960 | 3.6331 | 0.992 | 7.016 | 5120 | 6.514 | 0.3566 | 3 | AAL |
| SDSS J001020.25 − 103059.09 | 52141 | 0651 | 107 | 1.742540 | 2.5056 | 1.424 | 4.243 | 5045 | 4.993 | 0.2814 | 3 | AAL |
| SDSS J001029.92 − 101145.54 | 52138 | 0652 | 302 | 1.751640 | 3.2360 | 1.281 | 5.569 | 3665 | 2.994 | 0.6159 | 1 | Reg |
| SDSS J001053.58 + 000642.84 | 51795 | 0389 | 348 | 1.873370 | 2.6721 | 1.169 | 5.664 | 5655 | 7.185 | 0.2610 | 3 | Reg |
| SDSS J001054.41 − 085438.66 | 52141 | 0651 | 569 | 1.745720 | 9.3966 | 1.043 | 16.003 | 4485 | 7.364 | 0.7196 | 4 | Reg |
| SDSS J001111.14 + 151034.83 | 52251 | 0751 | 632 | 1.731630 | 2.7532 | 1.609 | 4.573 | 5700 | 6.602 | 0.2294 | 1 | Reg |
| SDSS J001142.79 + 152216.30 | 52251 | 0752 | 438 | 1.886190 | 3.6573 | 0.219 | 7.918 | 3270 | 2.812 | 0.9323 | 4 | Reg |
| SDSS J001157.76 − 103735.21 | 52138 | 0652 | 264 | 1.857680 | 4.2954 | 0.774 | 8.870 | 4060 | 4.573 | 0.6423 | 4 | AAL |
| SDSS J001244.62 + 141112.97 | 52251 | 0752 | 217 | 1.705560 | 3.2471 | 0.842 | 5.146 | 5660 | 6.881 | 0.2476 | 4 | AAL |
| SDSS J001330.58 + 001814.28 | 51795 | 0389 | 385 | 1.844230 | 1.8880 | 1.713 | 3.812 | 4270 | 3.401 | 0.3711 | 2 | Reg |
| SDSS J001341.74 + 143531.31 | 52251 | 0752 | 194 | 1.933230 | 1.8982 | 1.433 | 4.437 | 6480 | 8.412 | 0.1746 | 3 | AAL |
| SDSS J001400.45 + 004255.49 | 51795 | 0389 | 412 | 1.709720 | 4.5593 | 1.438 | 7.280 | 4045 | 4.137 | 0.5827 | 3 | Reg |
| SDSS J001408.23 − 085242.19 | 52138 | 0652 | 363 | 1.744560 | 4.5117 | 0.137 | 7.668 | 6825 | 12.068 | 0.2104 | 2 | BAL |
| SDSS J001411.00 − 084429.15 | 52138 | 0652 | 375 | 1.767220 | 2.9899 | 0.287 | 5.289 | 5470 | 6.510 | 0.2690 | 2 | AAL |
| SDSS J001438.28 − 010750.12 | 51795 | 0389 | 211 | 1.815640 | 4.8011 | 0.553 | 9.234 | 3295 | 3.070 | 0.9961 | 2 | BAL |
| SDSS J001453.37 − 002827.52 | 51795 | 0389 | 239 | 1.922620 | 3.7010 | 0.566 | 8.503 | 4405 | 5.278 | 0.5335 | 2 | Reg |
| SDSS J001507.00 − 000800.81 | 51795 | 0389 | 196 | 1.703300 | 10.1183 | 0.906 | 15.970 | 3020 | 3.336 | 1.5852 | 1 | Reg |
| SDSS J001545.33 − 095754.12 | 52138 | 0652 | 479 | 1.795910 | 1.3341 | 1.949 | 2.481 | 4780 | 3.483 | 0.2358 | 2 | Reg |
| SDSS J001657.00 + 005532.06 | 51900 | 0390 | 331 | 1.756100 | 3.0960 | 1.595 | 5.370 | 3775 | 3.123 | 0.5694 | 3 | Reg |
| SDSS J001710.85 + 135556.52 | 52251 | 0752 | 044 | 1.808170 | 10.4602 | 1.386 | 19.863 | 4360 | 7.704 | 0.8538 | 1 | AAL |
| SDSS J001741.85 − 105613.30 | 52138 | 0652 | 041 | 1.806080 | 3.6452 | 1.407 | 6.897 | 3555 | 3.115 | 0.7331 | 2 | Reg |
| SDSS J001800.21 + 004602.82 | 51795 | 0389 | 611 | 1.900380 | 3.3131 | 1.584 | 7.342 | 4690 | 5.583 | 0.4354 | 2 | Reg |
| SDSS J001826.80 − 091038.78 | 52138 | 0652 | 578 | 1.857870 | 2.9839 | 0.911 | 6.164 | 4105 | 3.940 | 0.5180 | 2 | Reg |
| SDSS J001913.57 − 103848.25 | 52138 | 0652 | 070 | 1.862490 | 2.2511 | 0.822 | 4.686 | 4245 | 3.704 | 0.4189 | 4 | Reg |
| SDSS J001959.48 − 090809.46 | 52145 | 0653 | 324 | 1.792750 | 1.4842 | 1.450 | 2.745 | 6195 | 6.135 | 0.1481 | 3 | Reg |
| SDSS J002000.50 + 155110.02 | 52233 | 0753 | 374 | 1.751000 | 1.9210 | 1.737 | 3.302 | 4470 | 3.484 | 0.3139 | 3 | AAL |
| SDSS J002028.35 − 002915.00 | 51900 | 0390 | 234 | 1.926880 | 2.7439 | 1.765 | 6.348 | 4165 | 4.112 | 0.5111 | 2 | AAL |
| SDSS J002028.97 + 153435.91 | 52233 | 0753 | 430 | 1.764390 | 4.2464 | 1.156 | 7.474 | 4035 | 4.168 | 0.5938 | 2 | AAL |
| SDSS J002127.88 + 010420.39 | 51900 | 0390 | 443 | 1.819400 | 4.9046 | 1.518 | 9.494 | 7615 | 16.610 | 0.1893 | 2 | BAL |
| SDSS J002132.63 − 092424.31 | 52145 | 0653 | 422 | 1.869800 | 2.8025 | 1.081 | 5.905 | 5690 | 7.419 | 0.2636 | 3 | Reg |
| SDSS J002143.30 + 010840.26 | 51900 | 0390 | 534 | 1.901220 | 2.2417 | 1.618 | 4.974 | 4790 | 4.850 | 0.3396 | 3 | Reg |
| SDSS J002302.56 + 153446.39 | 52233 | 0753 | 462 | 1.723460 | 3.2186 | 1.294 | 5.268 | 4790 | 4.983 | 0.3501 | 2 | BAL |
| SDSS J002344.36 + 143115.43 | 52233 | 0753 | 165 | 1.866000 | 5.4223 | 1.334 | 11.353 | 7715 | 18.544 | 0.2027 | 1 | BAL |
| SDSS J002411.66 − 004348.06 | 51782 | 0391 | 290 | 1.794470 | 6.6288 | 1.839 | 12.295 | 4575 | 6.770 | 0.6014 | 3 | AAL |
| SDSS J002439.64 − 091600.58 | 52145 | 0653 | 538 | 1.792960 | 3.5242 | 1.638 | 6.519 | 4625 | 5.135 | 0.4204 | 3 | Reg |
| SDSS J002448.07 − 090055.05 | 52145 | 0653 | 530 | 1.858650 | 3.2093 | 1.476 | 6.638 | 4510 | 4.924 | 0.4464 | 3 | Reg |

Note. — [The complete version of this table is in the electronic edition of the Astrophysical Journal and from http://physics.uwyo.edu/agn/. The printed edition contains only a sample.] Units on $F_\lambda$ are $10^{-17}$ erg cm$^{-2}$ s$^{-1}$ Å$^{-1}$. Units on $\lambda L_\lambda$ are $10^{45}$ erg s$^{-1}$. Both $F_\lambda$ and $\lambda L_\lambda$ are taken at 3000 Å. Units on the Mg II FWHM are km s$^{-1}$. Units on $M_{\rm BH}$ are $10^8\ M_\odot$.

Yamamoto, T. M., & Vansevičius, V. 1999, PASJ, 51, 405
York, D. G., et al. 2000, AJ, 120, 1579
Yuan, M. J., & Wills, B. J. 2003, ApJ, 593, L11
Zhou, H., Wang, T., Wang, H., Wang, J., Yuan, W., & Lu, Y. 2006, ApJ, 639, 716